Peptide-Modified Optical Filters for Detecting Protease Activity

Kristopher A. Kilian,[†] Till Böcking,[†,‡] Katharina Gaus,[§] Michael Gal,[‡] and J. Justin Gooding[†,*]

[†]School of Chemistry, [‡]School of Physics, and [§]Centre for Vascular Research, University of New South Wales, Sydney NSW 2052, Australia

ABSTRACT The organic derivatization of silicon-based nanoporous photonic crystals is presented as a method to immobilize peptides for the detection of protease enzymes in solution. A narrow-line-width rugate filter, a one-dimensional photonic crystal, is fabricated that exhibits a high-reflectivity optical resonance that is sensitive to small changes in the refractive index at the pore walls. To immobilize peptide in the pore of the photonic crystal, the hydrogen-terminated silicon surface was first modified with the alkene 10-succinimidyl undecenoate *via* hydrosilylation. The monolayer with the succinimide ester moiety at the distal end served the dual function of protecting the underlying silicon from oxidation as well as providing a surface suitable for subsequent derivatization with amines. The surface was further modified with 1-aminohexa(ethylene glycol) (EG_6) to resist nonspecific adsorption of proteins common in complex biological samples. The distal hydroxyl of the EG_6 is activated using the solid-phase coupling reagent disuccinimidyl carbonate for selective immobilization of peptides as protease recognition elements. X-ray photoelectron spectroscopy analysis reveals high activation and coupling efficiency at each stage of the functionalization. Exposure of the peptide-modified crystals to the protease subtilisin in solution causes a change in the refractive index, resulting in a shift of the resonance to shorter wavelengths, indicating cleavage of organic material within the pores. The lowest detected concentration of enzyme was 37 nM (7.4 pmol in 200 μL).

KEYWORDS: porous silicon · biosensor · photonic crystal · rugate filter · hydrosilylation · protease

Proteases are a critical component for many biological processes, and protease activity can be found in eukaryotic cells and tissues. The degree of proteolysis is related to many normal biological functions, such as cell migration and tissue remodeling, but has also been implicated in a host of pathologies.[1–3] Furthermore, proteases are common agents to many viruses and infectious diseases,[4–6] and as such their simple and timely detection is oftentimes critical. As a consequence, many schemes for detecting proteases in biological samples and tissues have been developed. Protease activity is predominantly detected by fluororescent methods,[7–12] but reports exist of methods based on calorimetric techniques,[13] radioactivity,[3] immunological assays,[14] and electrophoretic,[15] amperometric,[16] and optical methods.[17–21] However, many protease detection techniques require time-consuming sample preparation, which can reduce throughput and adversely affect the native activity of the enzymes. Furthermore, common transduction schemes (*i.e.* fluorogenic methods) require complicated laboratory equipment for read-out of activity, and many protease assays require overnight incubation times. The need for labels can also interfere with accurate protease detection by modifying the activity around the recognition sequence. To enable rapid and accurate assessment of protease activity, we report a label-free and portable approach that is more amenable to applications in the field (*i.e.*, bioterrorism prevention and point-of-care diagnosis).

Developments in nanoscience and technology have been a considerable resource for label-free detection schemes, with new materials and methods that enhance detection limits and simplify read-out.[18,19] Nanostructured optical materials have proven versatile tools for detecting biomolecular interactions.[18,20,21] In particular, devices fabricated with porous silicon (PSi) have shown promise, owing to the ease of fabricating one-dimensional photonic crystals.[22] PSi photonic crystals have a so-called "photonic bandgap" that confines reflected light to specific wavelengths. The porosity of the PSi determines the average refractive index and thus dictates the characteristics of the optical reflectance spectra. Small changes in the refractive index can lead to large shifts in the optical spectra. Exploiting this principle, shifting the optical response due to biomolecular binding in PSi photonic crystals has been demonstrated as an effective transduction mechanism for a range of biological events.[23–30] A significant benefit of biosensing with PSi photonic crystals is the label-free transduction by optical

See the accompanying Perspective by Sailor on p 248.

*Address correspondence to justin.gooding@unsw.edu.au.

Received for review August 2, 2007 and accepted October 09, 2007.

Published online October 31, 2007.
10.1021/nn700141n CCC: $37.00

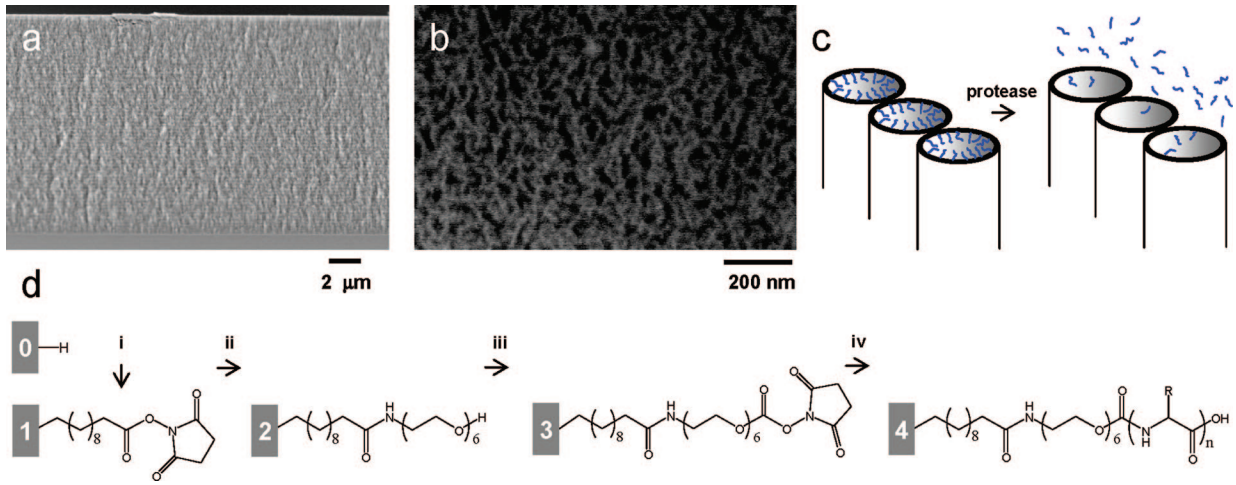

Figure 1. (a) Cross-section scanning electron microscopy image of a 60-layer PSi rugate filter. (b) Top view of the nanoporous surface. (c) Schematic illustration of immobilized substrate proteolysis at the pore tip. (d) Chemical scheme for biorecognition interface formation: surface 0, freshly etched PSi; surface 1, after hydrosilylation; surface 2, coupling of EG_6; surface 3, activation with DSC; surface 4, peptide immobilization ($n = 10$). Total layer thickness after derivatization is <5 nm, leaving ample pore space for infiltration of biomolecules.

interference (change in refractive index, *n*, within the film). Furthermore, remote read-out by using simple light sources independent of the material is possible.[28,31,32] Unfortunately, wide-scale employment of PSi for biological applications has suffered from the instability of the underlying surface to aqueous environments.[33,34] Similarly to an earlier report,[35] we recently modified the interior of PSi photonic crystals with a surface chemistry that allows mixing of biological fluids within the nanoporous framework while reducing nonspecific adsorption of competing biomolecules.[31,36] Importantly, the stability of the PSi was significantly enhanced such that collection of data for prolonged periods (up to two months) under physiological conditions is possible.[36] Previously, Orosco *et al.* demonstrated detection of protease on a porous silicon photonic crystal modified with protein on the top of the PSi structure.[18] The hydrophobic protein zein was spin-coated on the surface of an optical filter chemically modified internally with methyl termination. Digestion of the zein protein layer on the top of the PSi by a protease (pepsin) causes infiltration of protein fragments, thus making the pores hydrophilic and allowing the influx of water. The replacement of air in the pores with protein fragments and water results in a large shift in the optical resonance. While this is an exciting demonstration of photonic materials for detecting proteases, the generality of the approach suffers from the ill-defined nature of the zein protein substrate.

The purpose of this work is the demonstration of short-peptide immobilization on the interior of a photonic crystal for optical detection of protease activity. Organic functionalization of PSi rugate filters[37,38] is carried out using our recently reported surface protection strategy to promote biological stability.[31,36] Rugate filters, containing a sinusoidal variation of the refractive index normal to the growth axis, yield a narrow, high-reflectivity stop-band. The stop-band position is a function of the average refractive index in the crystal (n_{air} and $n_{silicon}$), thereby promoting shifts in the reflectivity as material infiltrates the photonic matrix ($n_{organic} > n_{air}$). Previously, photonic crystal transduction of chemical and biological events has relied on this "red-shift" to higher wavelengths for quantification.[23–28,31,36] The present study exploits the proteolytic hydrolysis of amide bonds, thus releasing material from the PSi interior ("blue-shift"), to transduce biorecognition of protease enzymes. The blue-shifting of the reflectivity by silicon oxidation has previously proven to be a major impediment to photonic crystal sensing[34,39] due to oxidation of the porous silicon surface. Hence, the sensing concept presented here is only possible because of the robust surface chemistry employed that effectively passivates the silicon surface from the ingress of water and hence protects the photonic crystal from surface oxidation.[31,36] In addition, inclusion of an antifouling hexa(ethylene glycol) (EG_6) moiety is necessary to prevent nonspecific adsorption of proteins that has been shown to accelerate oxidation and degrade the PSi.[31] All steps in the fabrication of the porous silicon device are characterized using X-ray photoelectron spectroscopy (XPS) in conjunction with reflectivity measurements. The sensor response to protease activity was verified by XPS and quantification of amino acids released into solution.

RESULTS AND DISCUSSION

Figure 1a shows a cross-sectional view of the entire 60-layer porous silicon (PSi) rugate filter after anodization using a sinusoidal current density. Figure 1b shows the resulting pore morphology at the top of the filter. At the applied current density, pore sizes of 50 nm are formed that will enable easy diffusion of biomolecules into the structure. Figure 1c schematically illustrates

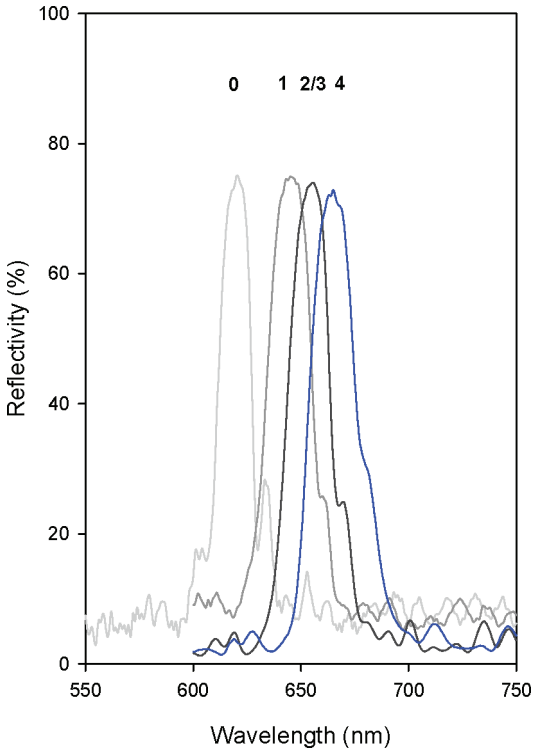

Figure 2. Reflectivity spectra of surfaces 0–4, indicating a red-shift in the optical filter reflectivity upon organic modification.

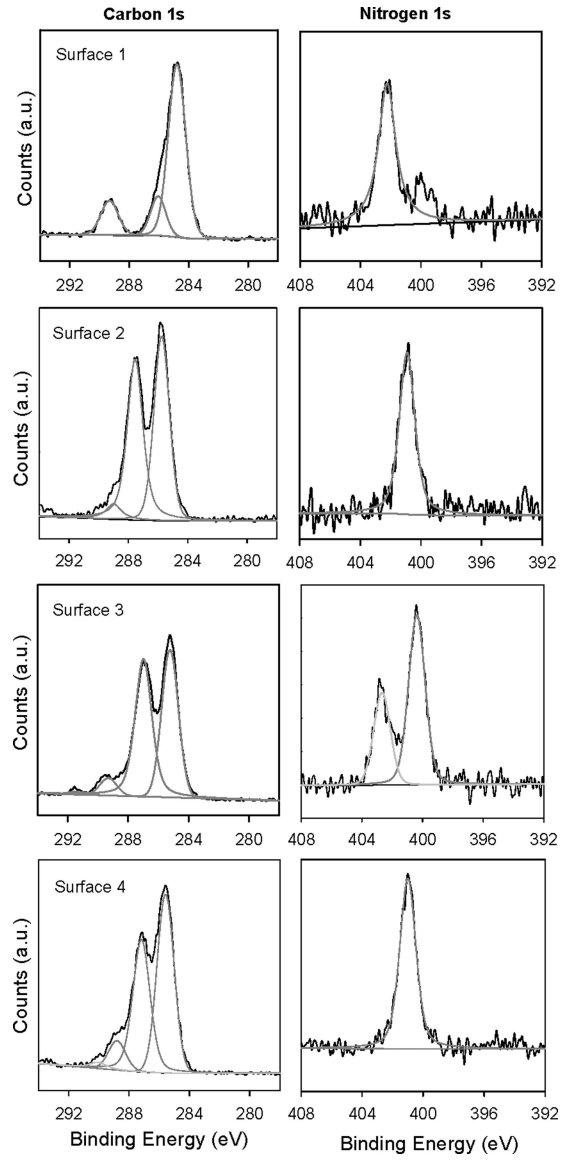

Figure 3. XPS narrow scans of the carbon 1s and nitrogen 1s regions for each of the surfaces 1–4 shown in Figure 1d.

peptide cleavage by protease enzymes within the pores of the material. Diffusion of peptide fragments out of the pores will cause a blue-shift in the position of the optical filter resonance for quantification of a proteolytic event. The scheme for forming the peptide biorecognition interface within the pores is depicted in Figure 1d: (i) Hydrosilylation of 10-succinimidyl undecenoate forms the base layer that protects the underlying silicon from degradation resulting from the ingress of water. (ii) Coupling of 1-aminohexa(ethylene glycol) (EG_6) provides an antifouling layer to resist nonspecific adsorption of proteins from biological samples. (iii) The distal hydroxyl functionality of the EG_6 layer could be activated using a strategy similar to that reported previously on flat silicon[40] using disuccinimidyl carbonate (DSC). (iv) The resultant succinimide carbonate group could subsequently be reacted with amines, such as those on biological molecules, to allow the immobilization of peptides *via* the formation of a carbamate bond.

Hydrosilylation of the alkene 10-succinimidyl undecanoate on the PSi rugate filters (surface 0→1) resulted in a 25 nm shift of the reflectivity peak (Figure 2), as expected for replacing air in the material with an organic layer. Coupling of the bioresistant EG_6 molecule resulted in an additional red-shift in the reflectivity of 10 nm (surface 2). Activation of the terminal hydroxyl group of the ethylene glycol layer with DSC gave no measurable shift, as expected (surface 3). Finally, incubation in a solution of the decapeptide (H_2N-AspArgValTyrIleHisProPheHisLeu-COOH, surface 4) resulted in the reflectivity being red-shifted an additional 10 nm. [Note: Reflectivity shifts were from a single experiment and are indicative of the typical magnitudes observed when modifying PSi rugate filters.]

The XPS survey spectrum at each step of derivatization indicates the presence of numerous peaks associated with the coupled biomolecules (Figure S1, Supporting Information). The silicon 2p and 2s photoelectron peaks from the PSi surface appear at ~100 and ~151 eV, respectively. After hydrosilylation (surface 1), the carbon 1s at ~286 eV, nitrogen 1s at ~401 eV, and oxygen 1s at ~533 eV are indicative of the contributions from 10-succinimidyl undecenoate. To systematically evaluate the chemical steps, narrow scans of the C1s and N1s regions were taken at each step to corroborate the optical reflectivity changes. The asymmetric peak at 285 eV in the C1s narrow scan (Figure 3, surface 1) was deconvoluted into two peaks. The

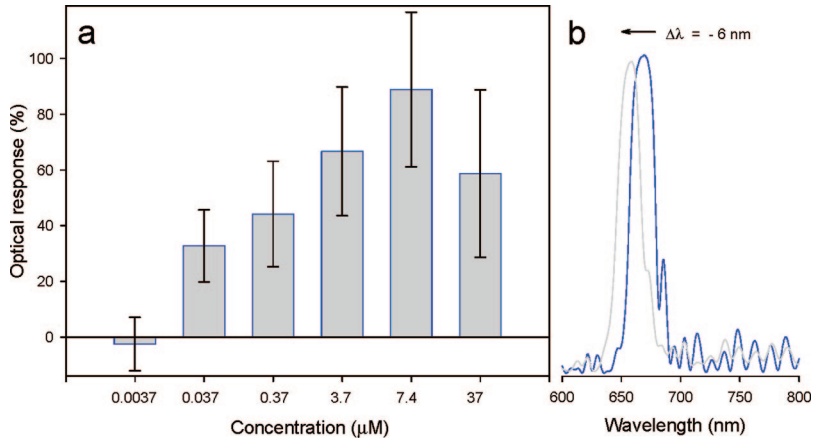

Figure 4. (a) Optical filter response ($(\Delta\lambda_{protease} - \Delta\lambda_{control}/\Delta\lambda_{peptide}) \times 100$) with respect to input enzyme concentration. (b) Representative reflectivity shift in the optical resonance after incubation in 3.7 μM enzyme. Error bars are the standard deviation of four experiments.

peak at ~284.8 eV is attributed to the aliphatic C–C carbons at the monolayer base, and the second peak at 286.0 eV is assigned to the contributions from carbons adjacent to carbonyl moieties. A higher binding energy peak at 289.3 eV was assigned to the carbonyl carbons of the ester and succinimide groups. The ratio of peak areas was 5:1:1 rather than the expected ratio of 3:1:1 (from molecule inspection), most likely due to hydrocarbon contamination on the surface, as suggested previously with similar organic layers on silicon.[41]

XPS analysis of the C1s narrow scan after coupling of the EG_6 moiety (Figure 3, surface 2) shows complete disappearance of the peak assigned to the succinimide group at 289.3 eV, indicating complete reaction of the amine with the active headgroups on the monolayer (with 13% hydrolyzed). The appearance of a peak at 287.5 eV is attributed to the C–O carbons of the ethylene oxide moieties. Additional evidence for reaction comes from the amide formed and adjacent carbons, assigned to a peak fitted at 289.0 eV. The ratio of the summed contributions from carbons shifted to higher binding energies (C–O of the EG_6, C–N of the EG_6, and carbonyl carbons of the amide group) to the alkyl C–C carbons at the base should be 13:10 for quantitative conversion of the NHS group to the amide. Peak areas result in a ratio of 11.4:10, which corresponds to 87% coupling of the EG_6 molecule. The N1s narrow scan was fitted with one peak at 400.4 eV assigned to the amide nitrogen. The high yield at this step is significantly larger than previous reports of amino coupling to NHS-terminated monolayers on flat silicon (40–50%).[41] The reason for the apparently high coupling efficiency on PSi is not clear but may be related to nanoscale topography with multiple silicon crystallite orientations and $Si–H_x$ ($x = 1, 2, 3$) configurations for Si–C bond formation. The combination of these effects may allow more reaction freedom (rotational, reduced steric demands) at the distal NHS.

Activation of the terminal hydroxyl group of the ethylene glycol layer with DSC has previously been shown as an efficient method to couple biological amines.[40] Figure 3, surface 3, shows the C1s and N1s narrow scans after activation. A new peak in the C1s at 291.4 eV is assigned to the carbonate carbon of the active moiety. The extent of activation from the C1s peak was difficult to quantitatively ascertain with the many species contributing to the same region of the spectrum. The N1s spectra displayed a new peak at 402.7 eV that was assigned to the succinimidyl nitrogen. Complete activation would result in a 1:1 ratio for these two nitrogen species. From the peak areas, 55% of the ethylene oxide chains were active, comparable to previous reports using this activation strategy (45%[40]).

The activated samples were then incubated in a solution of the peptide to complete fabrication of the biorecognition interface (Figure 3, surface 4). After immobilization, the C1s carbonate peak at 291.4 eV disappeared, with a new peak appearing at 290.1 eV, indicating successful reaction. This region was difficult to deconvolute and was subsequently attributed to a combination of amide bonds and carbamate linkages with contributions from arginine (1), histidine (2), and proline (1) side chains in the oligopeptide. Initially, the N1s displayed a small peak at 402.2 eV from remaining succinimide carbonate at the surface (19.7%, data not shown) which was hydrolyzed by incubation in KH_2PO_4 buffer at pH 7.9 for 4 h at 37 °C. From the N1s, the overall coupling efficiency of the oligopeptide to activated EG_6 chains is 64.1%. This equates to 35.2% of all the EG_6 chains at the interface actually having peptides coupled.

XPS analysis provides quantitative information about chemical modification at the surface of the PSi. To elucidate the penetration of the surface chemistry throughout the optical filter, all chemical derivatization steps were monitored with Fourier transform infrared spectroscopy to supplement the XPS characterization (Figure S2, Supporting Information). Appearance of organic modes indicative of each chemical step in conjunction with the XPS results and optical shifts of the filter reflectivity provides further evidence that organic layers have been formed throughout the complex nanoarchitecture.

The modified rugate filters were next exposed to enzyme solution. Subtilisin is a member of the serine endoproteinase family with a molecular weight of 27 kDa and a native size of $4.2 \times 4.2 \times 4.2$ nm^3. The small size of subtilisin means it can infiltrate into the pores of the rugate filters (pore diameter ~30–60 nm, Figure 1). Subtilisin has broad specificity with a preference for proteolysis of large uncharged residues. Digestion

of peptide by subtilisin after 4 h of incubation at 37 °C is evaluated by measuring the blue-shift in the reflectivity ($\Delta\lambda_{protease}$) as organic material is cleaved and replaced with air in the pores (Figure 4b). [Note: Coupling of short peptides results in relatively small shifts in the filter reflectivity (measured dry, <15 nm). When measured wet (water filling pore space), this shift is reduced roughly by a factor of 3 (<5 nm) such that detecting low concentration of enzyme requires drying the filter prior to reflectivity spectroscopy.] The optical response (% peptide digestion) is calculated by normalization to control ($\Delta\lambda_{control}$, buffer with no enzyme) and initial peptide ($\Delta\lambda_{peptide}$) reflectivity peak shifts: $(\Delta\lambda_{protease} - \Delta\lambda_{control}/\Delta\lambda_{peptide}) \times 100$. Figure 4a shows the optical response as a function of input enzyme concentration. Optical detection of protease activity was accomplished over a dynamic range of nanomolar to micromolar concentrations. The observed decrease in the optical response at 37 μM is most likely due to enzyme denaturation and adsorption at high concentrations within the filter, counteracting the expected blue-shift. To rule out any possibility that the presence of protein *per se* causes the blue shift rather than the specific peptide cleavage by active enzyme, an additional control using subtilisin inactivated by phenylmethyl - sulfonyl fluoride (PMSF) was performed. PMSF has been shown to inhibit proteolytic activity of serine proteases by >90%.[42] After 6 h at 37 °C, there was no difference between the buffer control and the inhibited enzyme, while active enzyme caused a complete blue-shift to the unmodified resonance position (Figure S3, Supporting Information). This result verifies that the observed optical response is due to proteolytic digestion.

To further verify that the optical sensor response was due to peptide digestion, XPS was performed to compare the control sample (– subtilisin) with the sample incubated in enzyme (3.7 μM). From the survey spectrum, a decrease in the carbon 1s peak is evident for the sample incubated in enzyme (with no change in the Si2s and Si2p peaks, Figure S4, Supporting Information). After initial peptide coupling, the carbon-to-silicon ratio from the C1s and Si2p narrow scans increased by 32%. After incubation with 3.7 μM subtilisin, the C1s:Si2p ratio at the surface of a rugate filter decreased 18.7%, indicating less carbon was present after enzyme digestion. The decrease of 18.7% means that 60% of the surface bound peptide has been digested by subtilisin. This estimate of the percentage of peptide digested is in close agreement to the optical response at 3.7 μM (67%, Figure 4a).

For accurate assessment of peptide cleavage within the porous network to supplement the XPS results, we investigated the quantity of amino acids released upon digestion using a ninhydrin reagent assay that detects free amino groups in solution by producing a colored product (absorbance at 570 nm), detectable by UV–vis spectroscopy. Aliquots of enzyme solution were removed and stored at –20 °C prior to, during, and after incubation with the PSi. Control solutions of enzyme were incubated under the same reaction conditions without rugate filters being present to account for amino acids liberated by cannibalism of subtilisin. The quantity of amino acids liberated in solution increases with protease concentration over the analyzed range (Figure 5). There is a clear trend for liberated amino acids with respect to enzyme concentration (Figure 5, solid triangles, $R^2 = 0.999$). Furthermore, the trend for enzyme concentration and optical response calculated by reflectivity shift completely coincides with the measured amino acids by ninhydrin (data offset for clarity, Figure 5, open circles, $R^2 = 0.998$). The agreement between subtilisin concentration and free amino acids in solution corroborates the optical data.

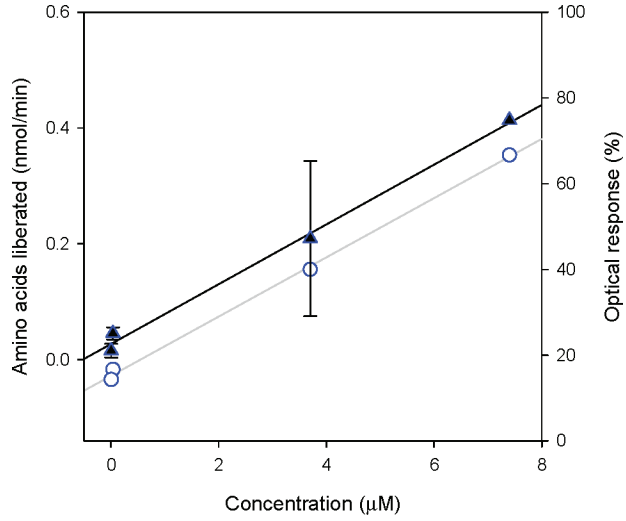

Figure 5. Liberated amino acids during incubation with different concentrations of enzyme (solid triangles, left axis; error bars are standard deviations from three experiments), and the corresponding optical response from the same samples used for the ninhydrin data (open circles, right axis).

Detection of low picomole amounts of protease (0.037 μM) is comparable to the approach developed by Sailor,[18] although longer incubation times are required to detect enzyme on the interior of the PSi. However, there are several advantages to detecting protease enzymes with our approach. Densely packed monolayers containing antifouling character allow small changes in the nanoporous matrix to be detected with minimal interference from oxidation or competing nonspecific biological effects. As a consequence, the improved stability will enable PSi photonic materials to be applied to problems where the complexity of the sample constituents has previously required cleanup. Furthermore, detecting low levels of analyte for extended times is plausible, allowing dynamic assays, *i.e.*, in clinical procedures or environmental monitoring. The use of functional alkenes and standard solid-phase coupling techniques provides unparalleled control over the molecular landscape such that, in future work, peptide sequences specific to cer-

tain proteases can be rationally incorporated to suit the application. Thus, the flexibility afforded with this approach will enable it to find utility for a host of sensing applications.

In conclusion, we have demonstrated for the first time covalent immobilization of complex peptides to the distal end of antifouling multilayers within the nanoporous framework of porous silicon photonic crystals. Instilling a robust chemical environment to the internal surface of rugate filters allows blue-shifts in the reflectivity to be detected upon substrate cleavage by protease enzymes. The generality of the approach and molecular-level control afforded should enable different chemical moieties to be incorporated for a variety of applications, thus expanding the scope of using photonic materials for sensing.

EXPERIMENTAL SECTION

Materials. All chemicals, materials, and reagents were purchased from Sigma-Aldrich (Sydney, Australia) unless otherwise specified. Solvents were redistilled prior to use, and mesitylene (1,3,5-trimethylbenzene) was redistilled from sodium and stored over molecular sieves. Milli-Q water (18 MΩ cm) was used for all buffer preparations and rinsing steps. p^+-type (boron-doped) Si(100) wafers (resistivity 0.005 Ω cm) were purchased from the Institute of Electronics Materials Technology (ITME, Warsaw, Poland). 10-Succinimidyl undecenoate was synthesized according to the procedure outlined in ref 41, and EG_6 was synthesized as described in ref 36.

Porous Silicon Rugate Filter Fabrication. Sixty-layer rugate filters with a sinusoidal porosity variation from 64 to 66% were prepared as described previously.[38] Briefly, silicon wafers (~1 cm^2) were back-contacted with a steel electrode and anodized with a platinum ring electrode in 25% ethanolic HF solution (equal parts 100% ethanol:50% HF). The current density profile during anodic etching was computer-controlled and included index matching at the air:PSi/PSi:Si interfaces, current breaks to reestablish electrolyte concentration at the dissolution front, and apodization of the waveform. After anodization, the porous silicon wafer was rinsed thoroughly with ethanol and pentane and dried under a stream of nitrogen.

Derivatization, Coupling, and Activation. Hydrosilylation was performed using Schlenck lines under argon as described previously.[36] Briefly, freshly etched samples were added to a solution of degassed (four freeze/pump/thaw cycles) 0.2 M 10-succinimidyl undecenoate in mesitylene and reacted overnight at 150 °C (12–24 h; surface 1). The modified samples were then incubated in 20 mM EG_6 in acetonitrile for 4 h (surface 2). Activation of EG_6-terminated samples occurred in a 0.1 M solution of DSC in dry acetonitrile (under molecular sieves) containing 0.1 M 4-dimethylaminopyridine for 8 h,followed by rinsing with ethyl acetate and CH_2Cl_2 (surface 3). Peptide immobilization occurred after incubating the activated sample with 1 mg/mL Angiotensin I in phosphate-buffered saline (PBS), pH 7.4, for 4 h, followed by rinsing with Milli-Q water, ethanol, and CH_2Cl_2 (surface 4).

Protease and Peptide Assays. Peptide-modified samples were placed in a glass vial with 0.001–10 mg/mL subtilisin (Sigma) in PBS and incubated at 37 °C for 4–6 h. After incubation, samples were rinsed with 37 °C Milli-Q water and placed in elution buffer (1×SSPE containing 1% 2-mercaptoethanol (v/v), 1% Triton X-100 (v/v), pH 7.4) at 37 °C for 1 h (to remove physisorbed enzyme). After elution, the samples were rinsed again with 37 °C Milli-Q water and 37 °C 100% ethanol, dried under a stream of argon, and measured. For the ninhydrin assay, standard curves were generated using 50 μM glycine in 0.05% glacial acetic acid (v/v) diluted to 0, 0.2, 0.4, 0.6, 0.8, 1, and 2 μM with 1% (v/v) ninhydrin reagent. Aliquots from the enzyme assay (with PSi rugate filters) were mixed with 1% ninhydrin, and all samples were heated at 100 °C for 10 min, followed by addition of 500 μL of ethanol (95%). Aliquots of 200 μL were then added to a quartz 96-well plate, and the absorbance was scanned between 500 and 600 nm ($\lambda_{max} \approx 570$ nm).

Subtilisin Inhibition. PMSF was dissolved in ethanol to 100 mM and further diluted to 2 mM in Tris buffer, pH 8.0. The 2 mM solution was added to subtilisin solutions 20% by volume and incubated for 60 min at room temperature prior to the protease assay.

X-ray Photoelectron Spectroscopy. X-ray photoelectron spectra were obtained using a EscaLab 220-IXL spectrometer with an Al Kα monochromated source (1486.6 eV), hemispherical analyzer, and multichannel detector. Spectra were recorded in normal emission with a spot size of 1 mm^2 and analyzing chamber pressure kept below 10^{-8} mbar. XPS data were analyzed using XPS-peak shareware.

Other Spectroscopies. Scanning electron micrographs were taken using a Hitachi S900 SEM with a 12 kV field emission source. The optical reflectivity spectra were measured at normal incidence using a J/Y SPEX 1681 spectrometer and silicon detector. The Fourier transform infrared spectra were collected with a ThermoNicolet AVATAR 370-FTIR spectrometer. Ninhydrin spectra were gathered using a Bio-Rad 96-well spectrophotometer.

Acknowledgment. The authors thank Suhrawardi Ilyas for assistance with rugate filter parameter optimization and the Australian Research Council for funding.

Supporting Information Available: Fourier transform infrared, X-ray photoelectron, and reflectivity spectroscopy data. This material is available free of charge *via* the Internet at http://pubs.acs.org.

REFERENCES AND NOTES

1. Proteases: New perspectives. In *Molecular and Cell Biology Updates*; Turk, V., Ed.; Birkhauser Verlag: Basel, Switzerland, 2001; pp 1–225.
2. Liaudet-Coopman, E.; Beaujouin, M.; Derocq, D.; Garcia, M.; Glondu-Lassis, M.; Laurent-Matha, V.; Prebois, C.; Rochefort, H.; Vignon, F. Cathepsin D: Newly Discovered Functions of a Long-Standing Aspartic Protease in Cancer and Apoptosis. *Cancer Lett.* **2006**, *237*, 167–179.
3. Hook, V. Y. H.; Schiller, M. R.; Nguyen, C.; Yasothornsrikul, S. Production of Radiolabeled Neuropeptide Precursors by In Vitro Transcription and Translation. *Pept. Res.* **1996**, *9*, 183–187.
4. Liang, P.-H. Characterization and Inhibition of SARS-Coronavirus Main Protease. *Curr. Top. Med. Chem.* **2006**, *6*, 361–376.
5. Scott, J. D. Simplifying the Treatment of HIV Infection with Ritonavir-Boosted Protease Inhibitors in Antiretroviral-Experienced Patients. *Am. J. Health-Syst. Pharm.* **2005**, *62*, 809–815.
6. Kido, H.; Okumura, Y.; Yamada, H.; Le, T. Q.; Yano, M. Proteases Essential for Human Influenza Virus Entry Into Cells and Their Inhibitors as Potential Therapeutic Agents. *Curr. Pharm. Des.* **2007**, *13*, 405–414.
7. Pinto, M. R.; Schanze, K. S. Amplified Fluorescence Sensing of Protease Activity with Conjugated Polyelectrolytes. *Proc. Natl. Acad. Sci. U.S.A.* **2004**, *101*, 7505–7510.
8. Eggeling, C.; Jaeger, S.; Winkler, D.; Kask, P. Comparison of Different Fluorescence Fluctuation Methods for Their Use in FRET Assays: Monitoring A Protease Reaction. *Curr. Pharm. Biotechnol.* **2005**, *6*, 351–371.
9. Gosalia, D. N.; Denney, W. S.; Salisbury, C. M.; Ellman, J. A.; Diamond, S. L. Functional Phenotyping of Human Plasma Using a 361-Fluorogenic Substrate Biosensing Microarray. *Biotechnol. Bioeng.* **2006**, *94*, 1099–1110.

10. Kaufmann, S. H.; Mesner, P. W., Jr.; Martins, L. M.; Kottke, T. J.; Earnshaw, W. C. Methods Used to Study Protease Activation During Apoptosis. In *Apoptosis in Neurobiology*; Hannun, Y. A., Boustany, R.-M., Eds.; CRC Press: Boca Raton, FL, 1999; pp 205–232.
11. Kohl, T.; Heinze, K. G.; Kuhlemann, R.; Koltermann, A.; Schwille, P. A Protease Assay for Two-Photon Crosscorrelation and FRET Analysis Based Solely on Fluorescent Proteins. *Proc. Natl. Acad. Sci. U.S.A.* **2002**, *99*, 12161–12166.
12. Eggeling, C.; Kask, P.; Winkler, D.; Jaeger, S. Rapid Analysis of Foerster Resonance Energy Transfer by Two-Color Global Fluorescence Correlation Spectroscopy: Trypsin Proteinase Reaction. *Biophys. J.* **2005**, *89*, 605–618.
13. Williams, B. A.; Toone, E. J. Calorimetric Evaluation of Enzyme Kinetic Parameters. *J. Org. Chem.* **1993**, *58*, 3507–3510.
14. Blair, I. S.; McDowell, D. A. Detection of Extracellular Proteinase of Pseudomonas fragi by Enzyme-Linked Immunosorbent Assay. *Curr. Microbiol.* **1995**, *31*, 180–185.
15. Frederiks, W. M.; Mook, O. R. F. Metabolic Mapping of Proteinase Activity with Emphasis on In Situ Zymography of Gelatinases: Review and Protocols. *J. Histochem. Cytochem.* **2004**, *52*, 711–722.
16. Ionescu, R. E.; Cosnier, S.; Marks, R. S. Protease Amperometric Sensor. *Anal. Chem.* **2006**, *78*, 6327–6331.
17. Wegner, G. J.; Wark, A. W.; Lee, H. J.; Codner, E.; Saeki, T.; Fang, S.; Corn, R. M. Real-Time Surface Plasmon Resonance Imaging Measurements for the Multiplexed Determination of Protein Adsorption/Desorption Kinetics and Surface Enzymatic Reactions on Peptide Microarrays. *Anal. Chem.* **2004**, *76*, 5677–5684.
18. Orosco, M. M.; Pacholski, C.; Miskelly, G. M.; Sailor, M. J. Protein-Coated Porous-Silicon Photonic Crystals for Amplified Optical Detection of Protease Activity. *Adv. Mater.* **2006**, *18*, 1393–1396.
19. Grant, S. A.; Weilbaecher, C.; Lichlyter, D. Development of a Protease Biosensor Utilizing Silica Nanobeads. *Sens. Actuators B* **2007**, *B121*, 482–489.
20. Millington, R. B.; Mayes, A. G.; Blyth, J.; Lowe, C. R. A Hologram Biosensor for Proteases. *Sens. Actuators B* **1996**, *B33*, 55–59.
21. Millington, R. B.; Mayes, A. G.; Blyth, J.; Lowe, C. R. A Holographic Sensor for Proteases. *Anal. Chem.* **1995**, *67*, 4229–4233.
22. Theiss, W. Optical Properties of Porous Silicon. *Surf. Sci. Rep.* **1997**, *29*, 91–192.
23. Pacholski, C.; Sartor, M.; Sailor, M. J.; Cunin, F.; Miskelly, G. M. Biosensing Using Porous Silicon Double-Layer Interferometers: Reflective Interferometric Fourier Transform Spectroscopy. *J. Am. Chem. Soc.* **2005**, *127*, 11636–11645.
24. Chan, S.; Horner, S. R.; Fauchet, P. M.; Miller, B. L. Identification of Gram Negative Bacteria Using Nanoscale Silicon Microcavities. *J. Am. Chem. Soc.* **2001**, *123*, 11797–11798.
25. Ouyang, H.; Christophersen, M.; Viard, R.; Miller, B. L.; Fauchet, P. M. Macroporous Silicon Microcavities for Macromolecule Detection. *Adv. Funct. Mater.* **2005**, *15*, 1851–1859.
26. Lin, V. S. Y.; Motesharei, K.; Dancil, K.-P. S.; Sailor, M. J.; Ghadiri, M. R. A Porous Silicon-Based Optical Interferometric Biosensor. *Science* **1997**, *278*, 840–843.
27. Schwartz, M. P.; Derfus, A. M.; Alvarez, S. D.; Bhatia, S. N.; Sailor, M. J. The Smart Petri Dish: A Nanostructured Photonic Crystal for Real-Time Monitoring of Living Cells. *Langmuir* **2006**, *22*, 7084–7090.
28. Kilian, K. A.; Böcking, T.; Gaus, K.; King-lacroix, J.; Gal, M.; Gooding, J. J. Hybrid Lipid Bilayers in Nanostructured Silicon: A Biomimetic Mesoporous Scaffold for Optical Detection of Cholera Toxin. *Chem. Commun.* **2007**, 1936–1938.
29. DeLouise, L. A.; Kou, P. M.; Miller, B. L. Cross-Correlation of Optical Microcavity Biosensor Response with Immobilized Enzyme Activity. Insights into Biosensor Sensitivity. *Anal. Chem.* **2005**, *77*, 3222–3230.
30. DeLouise, L. A.; Miller, B. L. Quantatitive Assessment of Enzyme Immobilization Capacity in Porous Silicon. *Anal. Chem.* **2004**, *76*, 6915–6920.
31. Kilian, K. A.; Böcking, T.; Ilyas, S.; Gaus, K.; Gal, M.; Gooding, J. J. Forming Antifouling Organic Multilayers on Porous Silicon Rugate Filters Towards In Vivo/Ex Vivo Biophotonic Devices. *Adv. Funct. Mater.* **2007**, *17*, 2884–2890.
32. Sailor, M. J.; Link, J. R. "Smart Dust": Nanostructured Devices in a Grain of Sand. *Chem. Commun.* **2005**, 1375–1383.
33. Tay, L.; Rowell, N. L.; Poitras, D.; Fraser, J. W.; Lockwood, D. J.; Boukherroub, R. Bovine Serum Albumin Adsorption on Passivated Porous Silicon Layers. *Can. J. Chem.* **2004**, *82*, 1545–1553.
34. Janshoff, A.; Dancil, K.-P. S.; Steinem, C.; Greiner, D. P.; Lin, V. S. Y.; Gurtner, C.; Motesharei, K.; Sailor, M. J.; Ghadiri, M. R. Macroporous p-Type Silicon Fabry-Perot Layers. Fabrication, Characterization, and Applications in Biosensing. *J. Am. Chem. Soc.* **1998**, *120*, 12108–12116.
35. Schwartz, M. P.; Cunin, F.; Cheung, R. W.; Sailor, M. J. Chemical Modification of Silicon Surfaces for Biological Applications. *Phys. Status Solidi A* **2005**, *202*, 1380–1384.
36. Kilian, K. A.; Böcking, T.; Gaus, K.; Gal, M.; Gooding, J. J. Si–C Linked Oligo(ethylene glycol) Layers in Porous Silicon Photonic Crystals: Optimization for Implantable Optical Materials. *Biomaterials* **2007**, *28*, 3055–3062.
37. Lorenzo, E.; Oton Claudio, J.; Capuj Nestor, E.; Ghulinyan, M.; Navarro-Urrios, D.; Gaburro, Z.; Pavesi, L. Porous Silicon-Based Rugate Filters. *Appl. Opt.* **2005**, *44*, 5415–5421.
38. Ilyas, S.; Böcking, T.; Kilian, K.; Reece, P. J.; Gooding, J.; Gaus, K.; Gal, M. Porous Silicon Based Narrow Line-Width Rugate Filters. *Opt. Mater.* **2007**, *29*, 619–622.
39. Steinem, C.; Janshoff, A.; Lin, V. S. Y.; Voelcker, N. H.; Reza Ghadiri, M. DNA hybridization-enhanced porous silicon corrosion: mechanistic investigations and prospect for optical interferometric biosensing. *Tetrahedron* **2004**, *60*, 11259–11267.
40. Böcking, T.; Kilian, K. A.; Hanley, T.; Ilyas, S.; Gaus, K.; Gal, M.; Gooding, J. J. Formation of Tetra(ethylene oxide) Terminated Si–C Linked Monolayers and Their Derivatization with Glycine: An Example of a Generic Strategy for the Immobilization of Biomolecules on Silicon. *Langmuir* **2005**, *21*, 10522–10529.
41. Böcking, T.; James, M.; Coster, H. G. L.; Chilcott, T. C.; Barrow, K. D. Structural Characterization of Organic Multilayers on Silicon(111) Formed by Immobilization of Molecular Films on Functionalized Si–C Linked Monolayers. *Langmuir* **2004**, *20*, 9227–9235.
42. Turini, P.; Kurooka, S.; Steer, M.; Corbascio, A.; Singer, T. The Action of Phenylmethylsulfonyl Fluoride on Human Acetylcholinesterase, Chymotyrpsin and Trypsin. *J. Pharmacol. Exp. Ther.* **1969**, *167*, 98–104.